EUROPEAN ORGANIZATION FOR NUCLEAR RESEARCH

Hyperfine structure of antiprotonic helium revealed by a laser-microwave-laser resonance method

E. Widmann[1] R.S. Hayano[1] T. Ishikawa[1] J. Sakaguchi[1] H. Yamaguchi[1] J. Eades[2]
M. Hori[2] H.A. Torii[3] B. Juhász[4] D. Horváth[5] T. Yamazaki[6]

ABSTRACT

Using a newly developed laser-microwave-laser resonance method, we observed a pair of microwave transitions between hyperfine levels of the $(n, L) = (37, 35)$ state of antiprotonic helium. This experiment confirms the quadruplet hyperfine structure due to the interaction of the antiproton orbital angular momentum, the electron spin and the antiproton spin as predicted by Bakalov and Korobov. The measured frequencies of $\nu_{\mathrm{HF}}^{+} = 12.89596 \pm 0.00034$ GHz and $\nu_{\mathrm{HF}}^{-} = 12.92467 \pm 0.00029$ GHz agree with recent theoretical calculations on a level of 6×10^{-5}.

(Submitted to Physical Review Letters)

[1] Department of Physics, University of Tokyo, 7-3-1 Hongo, Bunkyo-ku, Tokyo 113-0033, Japan
[2] CERN, EP Division, 1211 Genève 23, Switzerland
[3] Institute of Physics, University of Tokyo, Komaba, Meguro-ku, Tokyo 153-8902, Japan
[4] Institute of Nuclear Research of the Hungarian Academy of Sciences, H-4001 Debrecen, Hungary
[5] KFKI Research Institute for Particle and Nuclear Physics, H-1525 Budapest, Hungary
[6] RI Beam Science Laboratory, RIKEN, Wako, Saitama 351-0198, Japan

In this paper we report the first observation of microwave-induced transitions between magnetic substates of antiprotonic helium and use the results to determine its quadruplet hyperfine splitting to better than 1 MHz (relative precision $\sim 3 \times 10^{-5}$). Antiprotonic helium is an exotic three-body system consisting of a helium nucleus, an antiproton, and an electron ($\overline{p}-e^--\mathrm{He}^{2+} \equiv \overline{p}\mathrm{He}^+$). It has a series of highly excited metastable states (lifetime $\sim \mu\mathrm{s}$) with principal quantum number n and angular momentum quantum number L in the range 33–39, which have been extensively studied by laser spectroscopy (see [1, 2] and a comprehensive review [3]). In the most recent experiments performed at the CERN Antiproton Decelerator (AD), the wavelengths of several laser-induced transitions of the antiproton in $\overline{p}\mathrm{He}^+$ were measured with a relative accuracy of 1.3×10^{-7}, leading to a CPT test limiting any relative difference in the masses and charges of the proton and antiproton to 6×10^{-8} [4]. A step further in the precision spectroscopy of antiprotonic helium is the investigation of its magnetic *hyperfine structure*, i.e., the level splitting caused by the magnetic interaction of the $\overline{p}$ orbital angular momentum $\vec{L}_{\overline{p}}$, the electron spin $\vec{S}_e$, and the $\overline{p}$ spin $\vec{S}_{\overline{p}}$. To the leading order, the electron in $\overline{p}\mathrm{He}^+$ is in the ground state with a spin magnetic moment $\vec{\mu}_e = g_e\,\mu_\mathrm{B}\,\vec{S}_e$. The $\overline{p}$ magnetic moment, on the other hand, consists of an orbital part and a spin part $\vec{\mu}_{\overline{p}} = (g_\ell^{\overline{p}}\,\vec{L}_{\overline{p}} + g_\mathrm{s}^{\overline{p}}\,\vec{S}_{\overline{p}})\,\mu_{\overline{\mathrm{N}}}$. The orbital g-factor, $g_\ell^{\overline{p}}$, defines the relation between the $\overline{p}$ orbital magnetic moment and the anti-nuclear magneton $\mu_{\overline{\mathrm{N}}} = Q_{\overline{p}}\hbar/(2M_{\overline{p}})$. Its value is usually implicitly taken to be one, but this assumption has never been tested experimentally before, either for the proton or the antiproton.

Due to the large angular momentum of $\overline{p}\mathrm{He}^+$, the dominant splitting arises from the magnetic interaction of $\vec{S}_e$ with $\vec{L}_{\overline{p}}$. Thus, the coupling of $\vec{\mu}_{\overline{p}}$ with $\vec{\mu}_e$ creates a doublet (called here *hyperfine (HF) splitting*) with $\vec{F} = \vec{L}_{\overline{p}}+\vec{S}_e$ ($F^- = L-1/2$ and $F^+ = L+1/2$). The interaction of the $\overline{p}$ spin magnetic moment with the other magnetic moments splits each sublevel F^+ and F^- into a still finer doublet, and if $\vec{J} = \vec{F} + \vec{S}_{\overline{p}}$ is the total angular momentum, these further sublevels are associated with its components $J^{-+} = F^- +1/2 = L, J^{--} = F^- - 1/2 = L - 1, J^{++} = F^+ + 1/2 = L + 1$, and $J^{+-} = F^+ - 1/2 = L$. We refer to this as *superhyperfine (SHF) splitting*.

The theoretical framework of the hyperfine structure of $\overline{p}\mathrm{He}^+$ has been established by Bakalov and Korobov [5] who showed that the SHF splitting resulting from the one-body spin-orbit coupling of the antiproton ($\vec{L}_{\overline{p}}\cdot\vec{S}_{\overline{p}}$), and the scalar ($\vec{S}_{\overline{p}}\cdot\vec{S}_e$) and tensor ($(\vec{S}_{\overline{p}}\cdot\vec{S}_e)-3(\vec{S}_{\overline{p}}\times\vec{L}_{\overline{p}})\cdot(\vec{S}_e\times\vec{L}_{\overline{p}})/[L(L+1)]$) spin-spin couplings, yield the level order as shown in Fig. 1(a) due to an approximate cancellation of the latter two spin-spin coupling terms. Typical values for the HF splitting of metastable states are $\nu_\mathrm{HF} = 10 - 15$ GHz, while the SHF splitting is almost 2 orders of magnitude smaller ($\nu_\mathrm{SHF}^\pm = 150 - 300$ MHz). In a previous experiment at LEAR we indeed observed a doublet splitting of the unfavoured laser transition $(n, L) = (37, 35) \rightarrow (38, 34)$ at $\lambda = 726.1$ nm, the two sub-lines being separated by $\Delta = f_+ - f_- = \nu_\mathrm{HF}(\mathrm{initial})- \nu_\mathrm{HF}(\mathrm{final}) = 1.75 \pm 0.05$ GHz [6], in agreement with the theoretical value [5]. Although the SHF splitting is too small to be resolved with the pulsed laser system used in our experiments, it causes a small splitting of the hyperfine transition into two components, ν_HF^+ and ν_HF^- for $J^{-+} \leftrightarrow J^{++}$ and $J^{--} \leftrightarrow J^{+-}$, respectively, as shown in Fig. 1(a). In order to determine the two hyperfine frequencies of the $(37, 35)$ state on the MHz level directly, we developed the laser-microwave-laser resonance method described below.

The experiment was performed at the Antiproton Decelerator (AD) of CERN, which delivered pulses of $2 - 4 \times 10^7$ $\overline{p}$ of 200 ns length (FWHM) with a momentum of 100 MeV/c

(5.3 MeV kinetic energy). One such pulse was extracted from the AD every ~ 2 minutes and stopped in helium gas (see Fig. 2) at a temperature of 6.1 K and pressures of 250 or 530 mbar (number densities 3.0 or 6.7×10^{20} cm^{-3}, respectively). As described in further detail in Ref. [4], the time spectrum of delayed annihilations (ADATS, for Analog Delayed Annihilation Time Spectrum) was recorded in a digital oscilloscope as the envelope of the output of photomultipliers (PMTs) connected to two Čerenkov counters through which the antiproton annihilation products passed. Because 97% of antiprotons stopped in helium annihilate promptly (within picoseconds), the PMTs were turned off by a gate pulse until ~ 440 ns after the center of the AD pulse.

The wavy lines in Fig. 1(a) represent allowed M1 transitions (flipping $\vec{S}_e$ but not $\vec{S}_{\bar{p}}$) which can be induced by microwave radiation. All the HF levels are initially nearly equally populated. In order to create a population asymmetry which is needed to detect a microwave transition, a laser pulse stimulating a transition from a metastable ($\tau \sim \mu$s) state to a short-lived ($\tau \lesssim 10$ ns) state can be used. When the $\bar{p}$ is excited to the short-lived state, the $\bar{p}$He$^+$ undergoes an Auger transition to a $\bar{p}$He^{++} ion which is immediately destroyed via collisional Stark-effect in the dense helium medium followed by annihilation of the $\bar{p}$ with a nucleon. An on-resonance laser pulse therefore superposes a sharp spike onto the ADATS (cf. Fig. 3) whose area is proportional to the population of the metastable state at the time of the arrival of the laser pulse.

The laser-microwave-laser resonance method utilizes the following sequence: *i)* a laser pulse tuned to one of the doublet lines (e.g. f_+ in Fig. 1(a)) preferentially depopulates the F^+ over the F^- doublet. *ii)* The microwave pulse is applied; if it is resonant with either ν_{HF}^+ or ν_{HF}^-, it transfers population from the F^- to the F^+ doublet. *iii)* A second laser pulse at frequency f_+ measures the new population of F^+ after the microwave pulse.

The laser light of $\lambda = 726.1$ nm was produced by a commercial dye laser pumped by a Nd:YAG laser which was triggered synchronously with the arrival of the antiproton pulse. The line width of the dye laser with intra-cavity etalon was 0.6–0.8 GHz. A resonance scan (cf. Fig. 1(b)) showed a doublet structure with a separation of $\Delta = f_+ - f_- = 1.8 \pm 0.1$ GHz, in agreement with our earlier observation at LEAR [6]. The two sequential laser pulses were obtained by dividing the output of the dye laser and delaying one part by multiple reflections. In this way a maximum delay of 160 ns could be obtained without seriously degrading the laser beam spot quality. The laser power density was adjusted to achieve an optimum compromise between the depletion efficiency, i.e., the efficiency of depopulation of the F^+ doublet, and the power broadening which reduces the population asymmetry.

The Rabi frequency for the allowed microwave transitions is given by $\Gamma_{av} = \frac{1}{4\sqrt{2}} g_e \mu_B B_1$, where B_1 is the amplitude of the oscillating magnetic field. From this formula as well as from detailed numerical simulations [7, 8] it follows that in order to induce an M1 transition in the 160 ns time difference between the two laser pulses, a B_1 of several gauss is needed. To apply the microwave radiation, we constructed a cylindrical cavity for ν_{MW} ~ 12.9 GHz (diameter 28.8 mm, length 24.6 mm) resonating in the TM$_{110}$ mode. The ends of the cylinder were covered by metal meshes with a transparency of 85% permitting the $\bar{p}$ and the two laser beams to enter from opposite directions. The cavity was immersed in the low-temperature helium gas, and the microwave radiation was applied through a rectangular wave guide. An external triple stub tuner (TST) was used to tune the central frequency and Q-value of the cavity, thus allowing the microwave frequency to be scanned over a range of ~ 200 MHz corresponding to $\sim 1.5\%$ of the resonance frequency, while

keeping Q-values of ~ 2700 [8]. The resonance characteristics of the cavity were measured with a vector network analyzer (VNA) both in reflection and in transmission mode. The microwave pulse to induce the electron spin-flip transition was generated by amplifying the VNA output by a pulsed travelling wave tube amplifier (TWTA).

A measurement cycle consisted of the following computer-controlled steps. Before arrival of the antiprotons, the three stubs of the TST were set to obtain the desired resonance frequency and Q-value, and the cavity characteristics were verified using the VNA. The VNA was then tuned to this frequency, and upon arrival of the $\bar{p}$ beam, we fired the two laser pulses and the microwave pulse into the target. The ADATS of two Čerenkov counters showing two laser spikes each (cf. Fig. 3) were recorded.

We collected data during five 8-hour periods. At the beginning of each period, the laser alignment and depletion efficiency were verified. We then collected approximately 180–290 AD shots, stepping through 10–30 microwave frequencies in cycles. The microwave power was set to the optimum value (15 W) corresponding to an oscillating field strength of $B_1 = 7$ gauss inside the cavity as obtained from computer simulations. Each cycle included 1–3 points at very low microwave power for use as "microwave-off" reference points.

For each ADATS of one data taking period, we fitted a background function (a sum of two exponentials) to the time spectra in the range from 60 ns after the PMT was turned on to 500 ns after the first laser peak, excluding the two peak regions from the fit as shown in Fig. 3. We extracted the difference between the observed spectrum and the fit function in the two peak windows as shown in Fig. 3. The peak areas $I_+(t_i)$ are proportional to the population of the F^+ doublet at time t_i. In order to reduce systematic effects such as fluctuations in the overlap of laser and $\bar{p}$ beams or the $\bar{p}$ intensity, which might affect both peaks identically, we calculated the ratio $R^{++} \equiv I_+(t_2)/I_+(t_1)$ and plotted it against ν_{MW}. The individual data sets each showed two peaks at the theoretically predicted positions for ν_{HF}^+ and ν_{HF}^-. The off-resonance value of R^{++} agreed with the points taken at extremely low microwave power, but both varied from data set to data set. This results from uncontrollable systematic effects associated mainly with laser misalignments.

Each data set was fitted by a sum of two Lorentzian functions with identical width and amplitude, plus a constant background. The results for ν_{HF}^+ and ν_{HF}^- as well as the width of the Lorentzians agreed within the error bars and did not show any dependence on the target density. This is consistent with theoretical arguments presented by Korenman [9] that the shift of the line centres with density is very small, and that the collisional broadening at our densities is of the order of MHz.

We therefore normalized the individual data sets to the microwave-off value R_{off}^{++}, and averaged points within 0.7 MHz to give the final spectrum shown in Fig. 4. The chosen averaging interval was smaller than the line width $\gamma_{\mathrm{obs}} = 1/(2\pi\ 160\ \mathrm{ns}) = 1.0$ MHz corresponding to the 160-ns observation time window. The natural width of the $(37, 35)$ state of $\gamma_{(37,35)} = 0.12$ MHz is smaller than γ_{obs}, while the measured line width $\gamma_{\mathrm{exp}} = 5.3 \pm 0.7$ MHz was significantly larger. This may be due to collisions, to the inhomogeneity of the magnetic field over the stopping distribution of $\bar{p}$, or to the fact that the many substates with magnetic quantum numbers $m = -J \ldots J$ each have different Rabi frequencies.

The final results for ν_{HF}^+ and ν_{HF}^- obtained from fitting two Lorentzians plus a constant background to the spectrum of Fig. 4 are presented in Table 1 and compared to recent theoretical calculations by two groups. The theoretical values for for ν_{HF}^+ and ν_{HF}^- distribute over a much wider range (~ 100 ppm) than the laser transition energies

(~ 0.1 ppm) calculated by the same groups (see comparison in Ref. [4]), reflecting a higher sensitivity of the hyperfine coupling terms to the details of the wave functions involved. Nevertheless, the experimental values are in excellent agreement with the results of Korobov and Bakalov (both their initial values BK [5] and their most recent ones KB [10]) as well as the latest values of Kino *et al.* (K [11]).

In summary, we have established a laser-microwave-laser resonance method and succeeded in observing two microwave transitions, ν_{HF}^{+} and ν_{HF}^{-}, in antiprotonic helium. The experiment has fully confirmed the presence of a quadruplet structure originating from the hyperfine coupling of $\vec{L}_{\overline{p}}$, $\vec{S}_{e}$, and $\vec{S}_{\overline{p}}$, as predicted by Bakalov and Korobov [5]. The agreement of the experimental values ν_{HF}^{+} and ν_{HF}^{-} with the most updated theoretical values KB and K is about 6×10^{-5} or better, on the level of the accuracy of the calculations. These do not include contributions of order $\alpha^{2} \approx 5 \times 10^{-5}$ or higher. Presently, the experimental error is about 3×10^{-5}, slightly exceeding the theoretical precision. The microwave resonance frequencies, ν_{HF}^{+} and ν_{HF}^{-}, are primarily related to the dominant $\overline{p}$ orbital magnetic moment, which is probed by the aid of the large electron magnetic moment. As implied in the definition of $\vec{\mu}_{\overline{p}}$ (paragraph 1), ν_{HF}^{+} and ν_{HF}^{-} depend on the spin part $g_{s}^{\overline{p}}$ as well as on $g_{\ell}^{\overline{p}}$. This dependence is however too weak to permit a precise determination of $g_{s}^{\overline{p}}$, which would require a direct measurement of ν_{SHF}^{+} or ν_{SHF}^{-}. Thus, the excellent agreement between experiment and theory can be interpreted as an experimental measurement of the antiprotonic orbital g-factor with a relative precision of $\sim 6 \times 10^{-5}$. We note that no experimental value exists for g_{ℓ}^{p} for the proton because no atoms with an orbiting proton exist in the world of ordinary matter.

References

[1] M. Iwasaki *et al.*, Phys. Rev. Lett. **67**, 1246 (1991).

[2] T. Yamazaki *et al.*, Nature **361**, 238 (1993).

[3] T. Yamazaki, N. Morita, R. S. Hayano, E. Widmann, and J. Eades, Phys. Rep. **366**, 183 (2002).

[4] M. Hori *et al.*, Phys. Rev. Lett. **87**, 093401 (2001).

[5] D. Bakalov and V. I. Korobov, Phys. Rev. A **57**, 1662 (1998).

[6] E. Widmann *et al.*, Phys. Lett. B **404**, 15 (1997).

[7] J. Sakaguchi, Master's thesis, University of Tokyo, 2000.

[8] J. Sakaguchi *et al.*, (unpublished).

[9] G. Ya. Korenman (private communication).

[10] V. Korobov and D. Bakalov, J. Phys. B: At. Mol. Opt. Phys. **34**, L519 (2001).

[11] Y. Kino, N. Yamanaka, M. Kamimura, and H. Kudo, in *Proceedings of the 3rd European Conference on Atomic Physics at Accelerators (APAC2001)*, Aarhus, Denmark, 2001, Hyperfine Interactions, in press.

[12] N. Yamanaka, Y. Kino, H. Kudo, and M. Kamimura, Phys. Rev. A **63**, 012518 (2000).

Table 1: Experimental values for the HF transition frequencies of the state $(37, 35)$ in GHz compared to theoretical results. The relative experimental error δ_{exp} and the difference $\Delta_{\mathrm{th-exp}} \equiv (\nu_{\mathrm{th}} - \nu_{\mathrm{exp}})/\nu_{\mathrm{exp}}$ are given in ppm.

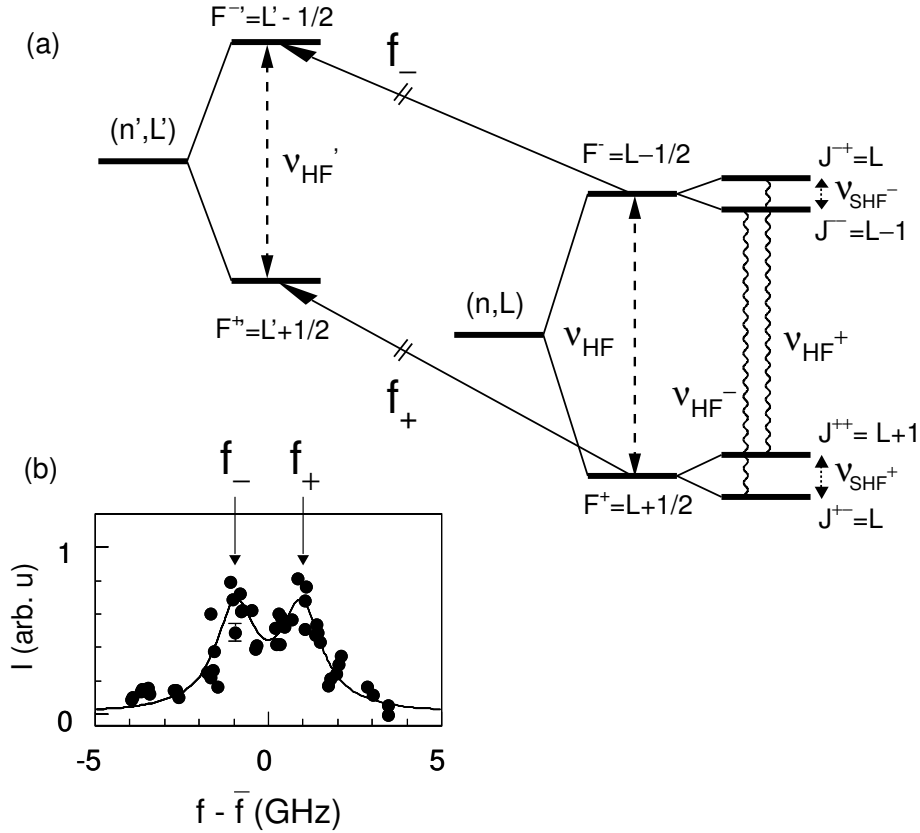|	ν_{HF}^{+} (GHz)	δ_{exp} (ppm)	ν_{HF}^{-} (GHz)	δ_{exp} (ppm)
Exp.	12.895 96(34)	27	12.924 67(29)	23
		$\Delta_{\mathrm{th-exp}}$		$\Delta_{\mathrm{th-exp}}$
BK [5]	12.895 97	0.6	12.923 94	-57
KB [10]	12.896 3462	30	12.924 2428	-33
YK [12]	12.898 977	234	12.926 884	171
K[11]	12.896 07391	8.6	12.923 96379	-55

Figure 1: (a) Schematic view of the splitting of a $\overline{p}\mathrm{He}^+$ state and observable laser transitions from the $F^\pm$ levels of a (n, L) state to a daughter state (n', L') (arrows). Wavy lines denote allowed magnetic transitions associated with an electron spin flip. (b) Laser scan of the 726.1 nm transition with $(n, L) = (37, 35)$ and $(n', L') = (38, 34)$ performed at the AD $(\overline{f} = (f_+ + f_-)/2)$.
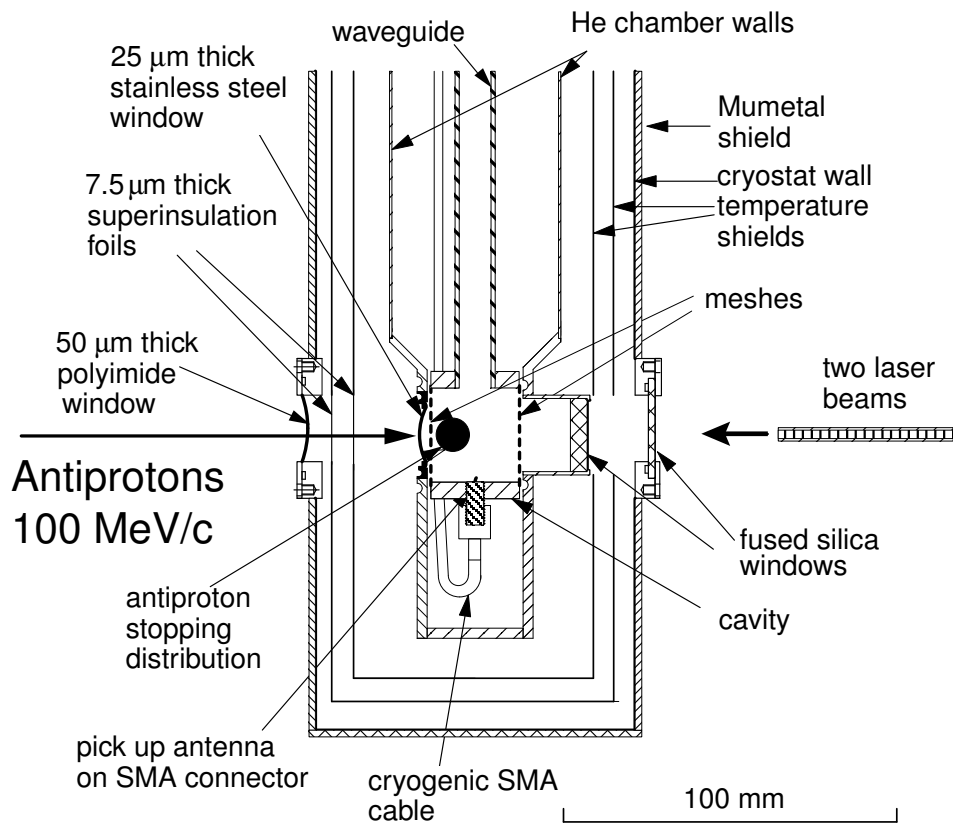
6

Figure 2: Side view of the cryostat holding the helium target chamber and microwave cavity. The antiprotons enter the helium chamber from left and stop inside a cylindrical microwave cavity. Two overlapping laser beams come from opposite direction along the cavity cylinder axis, and the microwave radiation is supplied through a rectangular wave guide from top. Two Čerenkov counters not shown in the drawing were placed on both sides of the cryostat where there is no window.
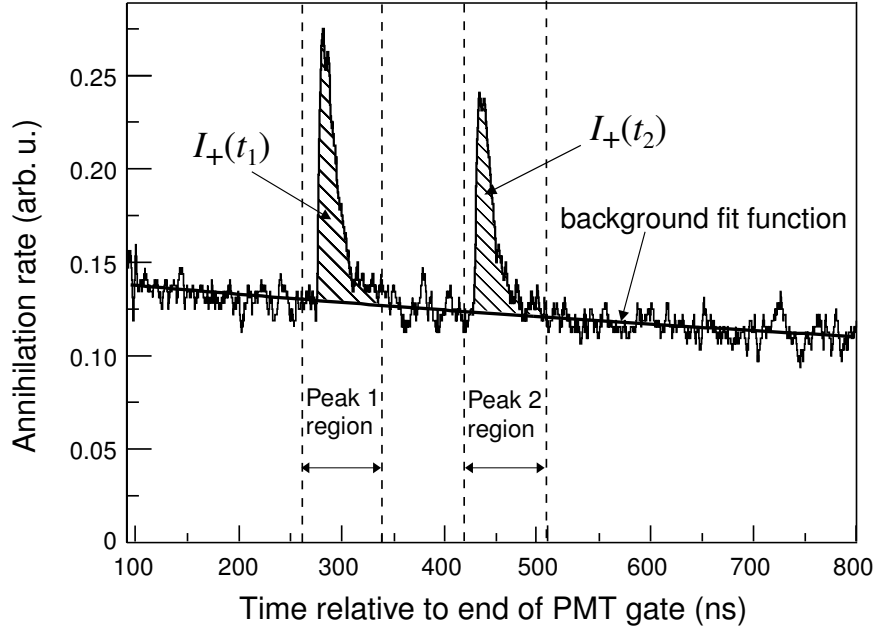
Figure 3: Part of ADATS with two successively applied laser pulses of frequency f_+. The background fit function and the two peak regions that are excluded from the background fit are also shown. $I_+(t_1)$ and $I_+(t_2)$ stand for the hatched areas under the two spikes.
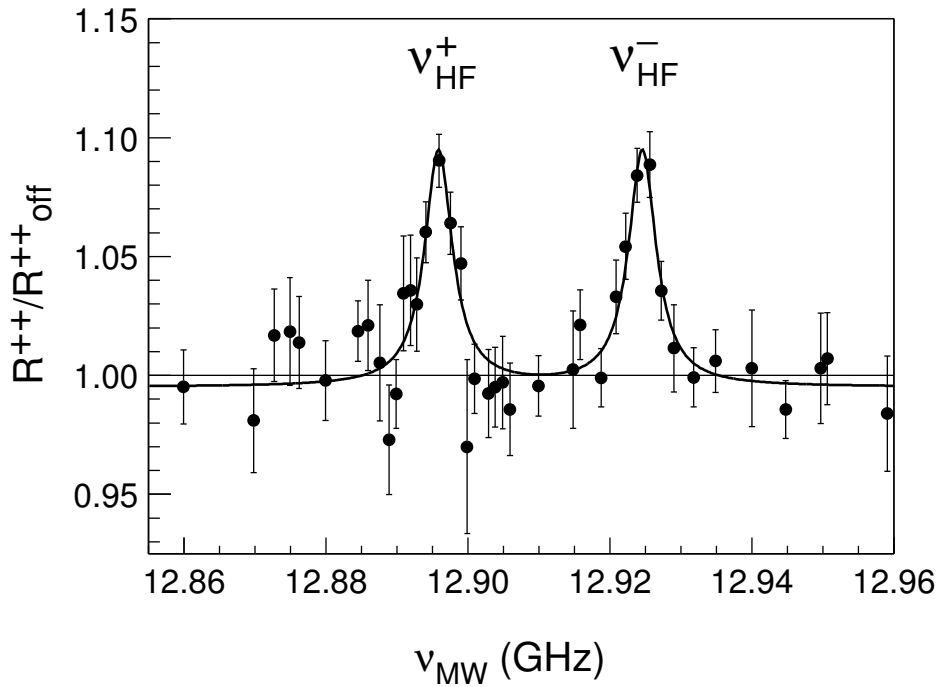

Figure 4: Average of all microwave scans showing clearly two resonance lines as predicted. The width of the lines of ~ 5 MHz corresponds to 4×10^{-4} of the central frequency.